DOI: 10.1002/cphc.201100593

Theoretical Study of the Raman Optical Activity Spectra of 3_{10}-Helical Polypeptides

Christoph R. Jacob*[a]

Raman optical activity (ROA) spectroscopy is a promising analytical method for studying the structure and conformation of polypeptides and proteins in solution. However, the structural information obtained from such vibrational spectra is only indirect and theoretical studies are often necessary to identify how the structure determines the observed spectra. One particular target is the identification and discrimination of different helical secondary structure elements. Herein, a theoretical investigation of the ROA spectra of a series of 3_{10}-helical polypeptides is presented. In particular, the effect of chain length, C^{α}-substitution pattern, the introduction of larger aliphatic side chains, and the variation of their conformation on the ROA spectra is studied. To extract general principles from these calculations, the positions, intensities, and shapes of the ROA bands are analyzed in terms of localized modes, which makes it possible to identify possible ROA signatures of 3_{10}-helical structures, but also provides fundamental insight into the generation of ROA signals in complex polypeptides. Finally, the calculated spectra can be compared to the previously reported ROA spectrum of a specifically designed 3_{10}-helical heptapeptide. This allows most of the features in the experimental spectrum to be assigned.

1. Introduction

The determination of the structure of biomolecules and the elucidation of biomolecular structure formation are at the core of a detailed understanding of biological functionality[1,2] and a prerequisite for the theoretical design of functional biomolecules (see, e.g. refs. [3], [4]). While X-ray diffraction is able to provide accurate structures for protein crystals, NMR spectroscopy can be employed to determine protein structures in solution. However, these well-established techniques are, in general, not suitable for studying the fast processes occurring in disordered and unfolded proteins, during protein folding, or while proteins perform their catalytic function. X-ray crystallography can only provide a static picture, whereas the time resolution of NMR spectroscopy is limited to microseconds because of the applied radio frequency pulses.[5,6]

Therefore, complementary spectroscopic techniques are necessary to investigate very flexible biomolecular structures and to elucidate fast structural changes during protein folding. One important tool is vibrational spectroscopy, which can be directly applied to proteins in their natural environment (i.e. in aqueous solution) and potentially provides femtosecond time resolution.[7,8] However, extracting structural information from vibrational spectra is a difficult task. First, conventional IR and Raman spectra of polypeptides and proteins are usually congested and contain a large number of transitions.[9–11] To overcome this problem, specialized spectroscopic techniques have been developed. In 2D IR spectroscopy,[12–15] the spectral information is spread out over two dimensions, which provides access to anharmonic couplings between different vibrations. Other techniques such as resonance Raman spectroscopy[16–20] or the chiral variants of IR and Raman spectroscopy,[21] vibrational circular dichroism (VCD),[22] and Raman optical activity (ROA),[23–25] filter specific information. Second, the relationship between vibrational spectra and molecular structure is only indirect and quantum chemical calculations are often indispensable for extracting structural information.[26]

To elucidate the structures of unfolded or disordered protein structures in solution, one important task is to distinguish between different helical conformations. Chiral vibrational spectroscopy is a valuable tool for this task. For instance, VCD spectroscopy is able to distinguish α- and 3_{10}-helical polypeptide conformations[27,28] and ROA spectroscopy has been employed to elucidate the solution structure of polypeptides adopting the poly(L-proline) II conformation.[29,30] Herein, ROA spectroscopy, which is particularly sensitive to structural differences in unfolded and disordered proteins is focused upon.[31–34] However, a detailed understanding of the relationship between helical structure and ROA spectra, as well as simple rules of thumb for the rationalization of polypeptide ROA spectra, are still not available. Therefore, dedicated computational studies are necessary to be able to reliably assign signatures of different helical conformations (see, e.g. refs. [35]–[39]).

To this end, a theoretical study of the ROA spectra of helical polypeptides containing twenty alanine (Scheme 1) residues was recently performed.[37] By combining DFT calculations with an analysis in terms of localized modes,[40,41] it was possible to obtain a detailed understanding of the different bands observed in the ROA spectra. In particular, it was possible to assign vibrations responsible for each of the bands and to identify the mechanisms by which the ROA intensities and band shapes arise. This made it possible to extract relation-

[a] *Dr. Ch. R. Jacob*
Karlsruhe Institute of Technology (KIT)
Center for Functional Nanostructures (CFN)
Wolfgang-Gaede-Str. 1a
76131 Karlsruhe (Germany)
E-mail: christoph.jacob@kit.edu

Supporting information for this article is available on the WWW under http://dx.doi.org/10.1002/cphc.201100593.

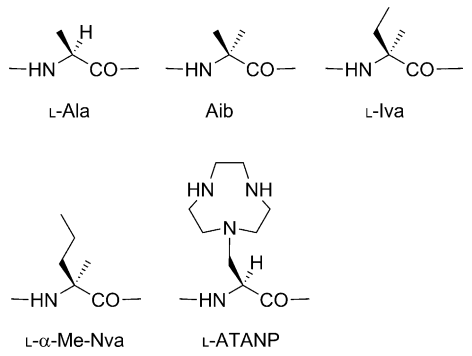

Scheme 1. Lewis structures of the amino acid building blocks considered.

ships between the α- and 3_{10}-helical backbone structure—in particular, the different hydrogen-bonding pattern—and the ROA spectra and allowed signatures that are specific to these helical conformations to be proposed.

However, while, for α-helical alanine polypeptides, a comparison of the computational results with measured spectra of polyalanine, as well as other α-helical polypeptides,[42] is possible and confirms the proposed signatures,[37] a comparison to experimental data for the 3_{10}-helical conformation is more difficult. Even though signatures of 3_{10}-helices, for instance, a positive ROA signal at 1340 cm^{-1}, were previously proposed based on a comparison of the measured ROA spectra of different proteins containing 3_{10}-helices, among other secondary structure elements,[43,44] such assignments are often ambiguous. In many cases, it is not clear which structural features are responsible for the experimentally observed ROA bands, and consequently, the proposed signatures of 3_{10}-helices were revised in subsequent work.[31]

Thus, experimental ROA studies on model polypeptides known to adopt a single, well-defined conformation are required for a meaningful comparison of experimental and theoretical work. However, polypeptides made from alanine or other standard α-amino acids do not adopt a 3_{10}-helical conformation. To obtain a 3_{10}-helix, C^{α}-tetrasubstituted amino acids need to be introduced and it is also necessary to employ larger aliphatic side chains to achieve a preference for right-handed helices. In addition, more complex side chains, for instance, containing a triazacyclononane (TAN) ring, are required to obtain water-soluble polypeptides.[45–48] The ROA spectrum of such a specifically designed 3_{10}-helical heptapeptide was reported by Toniolo et al.[49] To be able to compare calculated ROA spectra with this experimental spectrum, it has to be investigated how both C^{α}-tetrasubstitution and the variation of the amino acid side chains affect the ROA spectra.

Herein, a systematic computational study of the ROA spectra of 3_{10}-helical polypeptides is presented. In particular, it is investigated how the chain length, the C^{α}-substitution pattern, and variations of the side chains affect the calculated ROA spectra of 3_{10}-helical polypeptides. This is not only important for identifying ROA signatures of helical structures, but also provides further insight into mechanisms determining the ROA spectra of polypeptides in general and provides valuable insight for the assignment and interpretation of polypeptide ROA spectra.

This work is organized as follows: The theoretical background of the calculation of ROA spectra and their analysis in terms of localized modes is summarized and the mechanisms determining the intensities and band shapes in polypeptide ROA spectra are briefly reviewed. This is followed by a discussion of the ROA spectra of 3_{10}-helical Ala_{20} polypeptides and the previously proposed signatures of 3_{10}-helices. Next, the model structure setup is discussed. This is followed by the computational results and the effect of the chain lengths, the C^{α}-substitution pattern, and the variation of the identity and the conformation of the amino acid side chains are analyzed. Finally, a comparison to experimental spectra is drawn.

2. Theoretical Background

Within the harmonic approximation, the normal modes $\boldsymbol{Q}$ and the corresponding vibrational frequencies are obtained by diagonalizing the mass-weighted Hessian matrix $\boldsymbol{H}^{(m)}$.[26,50] For the pth normal mode, $\boldsymbol{Q}_p$ with vibrational frequency ν_p, the ROA intensities are—within the commonly employed semiclassical framework and assuming a nondegenerate ground state and that the incident laser light is not in resonance with an electronic excitation of the molecule[23,51]—determined by the ROA invariants $\beta(\boldsymbol{G}')^2_p$ and $\beta(\boldsymbol{A})^2_p$, which in turn depend on the derivatives of the electric dipole–electric dipole polarizability tensor, α, the electric dipole–magnetic dipole polarizability tensor, $\boldsymbol{G}'$, and the electric dipole–electric quadrupole polarizability tensor $\boldsymbol{A}$ with respect to the normal mode, $\boldsymbol{Q}_p$. These polarizability tensors can be calculated by using response theory, most commonly time-dependent DFT,[52,53] and their derivatives are accessible either with numerical[54–56] or analytical[57–60] derivative techniques. Details on the computational methodology employed herein are summarized in the Computational Methodology Section.

For large molecules, such as the polypeptides considered in this work, the calculated vibrational spectra feature a large number of close-lying normal modes. These individual vibrational transitions are not resolved in experiment and only bands to which several normal modes contribute are observed. These bands can be characterized by their position (i.e. the frequency or wavenumber at which they appear in the spectrum), their total intensity (i.e. the intensity integrated over the whole band, which is equal to the sum of the intensities of the individual transitions), and their band shape (i.e. whether a single peak, a couplet, or a more complicated band shape is observed). Thus, to relate calculated spectra to experimental data, it is not useful to consider the individual normal modes, but rather one needs to understand how these bands arise and how their positions, intensities, and shapes are determined.

This can be achieved by performing an analysis in terms of localized modes.[40] For such an analysis, one considers the subset of normal modes, $\boldsymbol{Q}^{\mathrm{sub}}$, contributing to one band. For this subset, one performs a unitary transformation, $\boldsymbol{U}$, which is determined such that the resulting transformed modes, $\tilde{\boldsymbol{Q}}^{\mathrm{sub}} = \boldsymbol{Q}^{\mathrm{sub}}\boldsymbol{U}$, are as localized as possible when measured by a suitable localization criterion.[40] Here and in the following, a tilde is

used to denote all quantities that refer to localized modes. In contrast to the normal modes, which are delocalized over the whole polypeptide, these localized modes are, in general, dominated by a vibration of one single amino acid residue. In addition, the localized modes obtained for one vibrational band are similar to each other and feature similar atomic displacements on the different residues.

Even though the Hessian matrix with respect to the localized modes, $\tilde{\boldsymbol{H}}^{sub}$, is not diagonal, its diagonal elements can be used to assign frequencies, $\tilde{\nu}_p$, to the localized modes. To first order, these local mode frequencies are related to the band positions. Furthermore, vibrational intensities of the localized modes can be defined by considering the derivatives of the required polarizability tensors with respect to the localized modes. It can be shown that the total intensity of one band is invariant under a unitary transformation of the contributing modes[40] and, therefore, the intensities of the localized modes directly determine the total band intensities. Since the localized modes obtained for one band are, in general, similar, they usually show similar frequencies and intensities, so that the band positions and their total intensities can be understood by considering only one representative localized mode.[40,41]

In the case of ROA spectra, two different mechanisms can be identified that give rise to local mode intensities, and thus, the total intensities of ROA bands.[37] First, in a chiral molecule, a vibration of a single, achiral group can have a nonvanishing ROA intensity. In this case, the ROA intensity is caused only by the electronic chirality, that is, the chirality of the electronic structure is probed by an achiral vibration.[61] This is, for instance, the case for the amide I band (which is due to the stretching vibrations of the amide C=O group)[37] in polypeptides or for the W3 vibration of tryptophan side chains.[62] Second, the arrangement of the vibrating atoms can be chiral by itself, so that the ROA intensity arises due to vibrational chirality. Usually such vibrations can be described as coupled vibrations of two (or more) achiral groups and their ROA intensity depends on the orientation of these groups with respect to each other. This makes the total intensities of the corresponding ROA bands very sensitive to structural changes. The vibrations in the extended amide III region in polypeptides are an important example of this second type.[37,63] Further examples of these two different mechanisms are discussed in more detail in the following section.

To understand the shapes of ROA bands, considering only the frequencies and intensities of the contributing localized modes is not sufficient; in addition, the coupling between the localized modes also has to be taken into account. The vibrational coupling matrix, $\tilde{\Omega}$, which is related to the Hessian matrix with respect to the localized modes, $\tilde{\boldsymbol{H}}^{sub}$,[40] determines how the localized modes couple to normal modes. Because the localized modes are similar to each other, this coupling matrix usually has a simple structure and its elements only depend on the distance between the corresponding localized modes. The distribution of the intensity among the resulting normal modes is then determined by the elements of the intensity coupling matrix, $\left[\tilde{\boldsymbol{I}}\right]$, which are given by products of the polarizability tensor derivatives with respect to localized modes. For definitions and a more detailed discussion, see references [37], [41].

For ROA band shapes, two important cases can be distinguished.[37] If either the vibrational coupling constants or the intensity coupling constants (or both) are small, a single peak is obtained. If, on the other hand, the nearest-neighbor intensity coupling constants are large and if in addition the vibrational coupling constants do not vanish, a couplet arises. The orientation of this couplet (i.e. whether it is positive at low wavenumbers and negative at high wavenumbers or the other way around) then depends on the signs of the nearest-neighbor intensity coupling constants and the largest vibrational coupling constants. Additionally, more complicated coupling patterns are also possible.[37,64]

3. ROA Spectra of 3_{10}-Helical Alanine Polypeptides

To provide a starting point for the analysis and discussion of the calculated ROA spectra of more complicated 3_{10}-helical polypeptides, the results obtained previously for 3_{10}-helical Ala_{20} are briefly reviewed.[37] The calculated ROA spectrum is shown in Figure 1 a, in which the assignment of the individual normal modes to bands is also indicated.

To identify the vibrations responsible for each of these bands, one can consider a representative localized mode (i.e. a localized mode on a residue in the center of the helix). Except for possible deviations occurring at the ends of the helix, in all cases very similar atomic displacements are found for all localized modes. Because only atoms of one residue contribute significantly, these representative localized modes can be visualized by only showing the atoms of one residue, as in Figure 1 b.

The amide bands are those that are related to vibrations of the peptide bonds between the amino acid residues. The amide I band between 1630 and 1660 cm^{-1} is mainly caused by a stretching vibration of the C=O group, with smaller contributions of a bending vibration of the adjacent N–H group. The amide II band between 1470 and 1520 cm^{-1} is due to an out-of-phase combination of the C–N stretching vibration and the N–H bending vibration. The amide III band at 1180–1250 cm^{-1} is the corresponding in-phase combination (which can be referred to as the "classical" amide III vibration) that mixes with C^{α}–H bending vibrations. It is usually discussed together with the two bands at 1300–1330 and at 1260–1290 cm^{-1}, which are due to the two C^{α}–H bending vibrations (in the direction of the N–C^{α} band and perpendicular to it, respectively), which in turn mix with the classical amide III vibration. The amide III and the two C^{α}–H bending bands together form the extended amide III region.

In addition, there are bands between 1340 and 1460 cm^{-1} that are related to vibrations of the methyl groups in the alanine side chains. The band at 1367 cm^{-1} is due to the symmetric CH_3 bending vibration, whereas the one at around 1460 cm^{-1} is caused by the two asymmetric CH_3 bending vibrations. Finally, the region between 1000 and 1200 cm^{-1} fea-

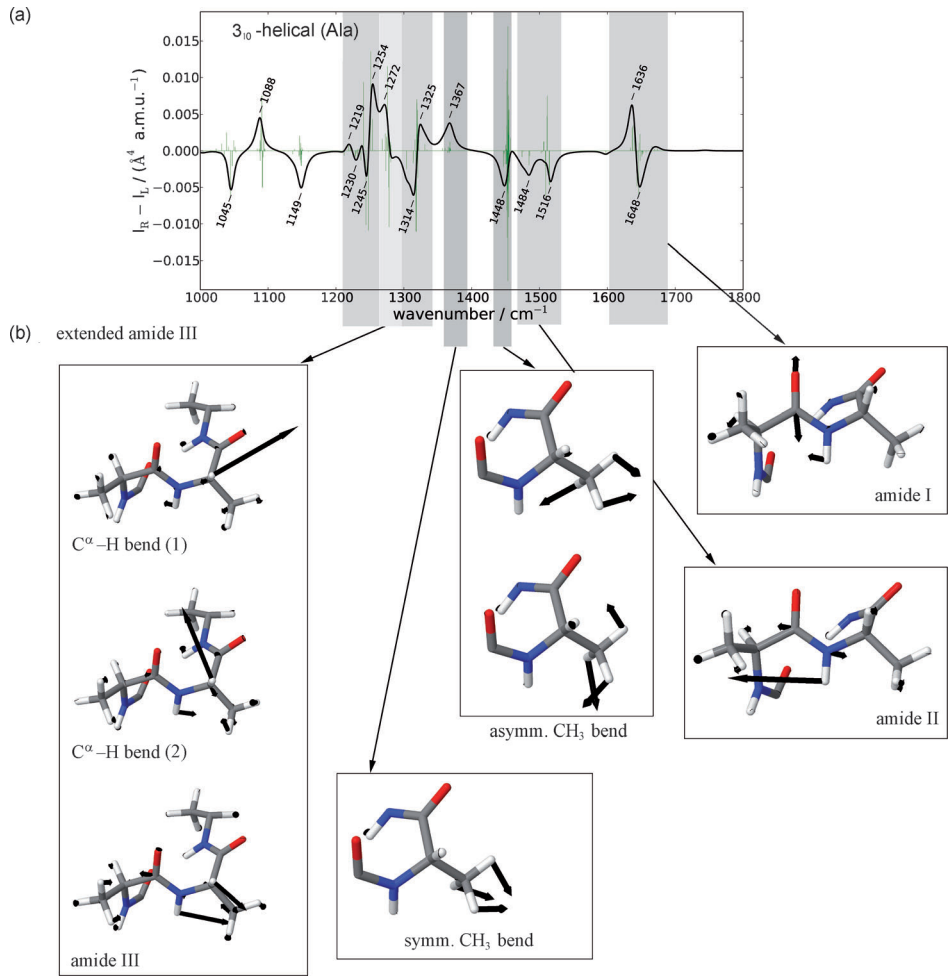

Figure 1. a) Calculated ROA spectrum of 3_{10}-helical $(Ala)_{20}$,[37] including the assignments of the different bands. The spectra have been plotted by using a Lorentzian line width of 15 cm^{-1} and the individual transitions have been included as a line spectrum scaled by 0.04. b) Representative localized modes for each of the bands in the calculated ROA spectrum of 3_{10}-helical $(Ala)_{20}$. Only those atoms that contribute significantly are shown.

tures C$^\alpha$–N and C–C stretching vibrations. However, a detailed discussion of this spectral region is omitted herein.

By analyzing the localized modes, it is possible to identify the mechanisms that determine the total ROA intensities and the shapes of the bands in the calculated ROA spectrum.[37] The localized modes obtained for the amide I and amide III bands, as well as the CH_3 bending bands, are vibrations of achiral groups, and hence, the total ROA intensities of these bands are due to electronic chirality only. On the other hand, in the extended amide III region, the total ROA intensities of the two C$^\alpha$–H bending bands and of the amide III band are due to vibrational chirality. The corresponding localized modes are chiral by themselves because of mixing between the classical amide III vibration and the C$^\alpha$–H bending vibrations.

Through comparison with the calculated ROA spectrum of α-helical Ala_{20}, possible signatures of 3_{10}-helical structures were identified in reference [37]. First, the couplet found for the amide I band is positive at low wavenumbers and negative at high wavenumbers, which is opposite to the amide I couplet found in α-helical polypeptides. This can be directly related to the different hydrogen-bonding patterns. While in an α helix the positive nearest neighbor coupling constant of about +8 cm^{-1} is the largest in magnitude, and thus, determines the vibrational coupling, for the 3_{10}-helix the negative second-nearest coupling constant has the largest magnitude (ca. −3.7 cm^{-1} vs. ca. +2.7 cm^{-1} for the nearest-neighbor coupling). This decrease of the nearest-neighbor coupling is related to the different relative orientations of the C=O groups, whereas the increase of the second-nearest-neighbor coupling is due to the hydrogen bond between the corresponding peptide units. Since the sign of the dominating vibrational coupling constants changes while the intensity coupling matrix remains similar, one obtains a reverse amide I couplet. These different vibrational coupling patterns for α- and 3_{10}-helical polypeptides have recently also been confirmed experimentally by careful isotopic substitution studies.[65]

Second, the total ROA intensity of the amide II band increases for the 3_{10}-helical polypeptide compared to the α helix, for which the amide II band is not visible. Due to a significant nearest-neighbor vibrational coupling constant of around −6.2 cm^{-1} (compared to ca. −2.8 cm^{-1} for the α helix), in combination with an intensity coupling matrix in which the nearest-neighbor contributions almost vanish, this amide II band splits into two peaks at 1484 and 1516 cm^{-1}.

In addition, several differences are also found in the extended amide III region. Because of coupling between the classical amide III vibration and the C$^\alpha$–H bending vibrations, these bands are very sensitive to structural changes. This coupling is also strongly affected by solvent effects and, therefore, more detailed studies, including explicit solvation, are required to make reliable predictions for these bands. Finally, for the CH_3 bending localized modes, similar wavenumbers and ROA intensities are obtained for the α- and 3_{10}-helical conformations, but the two peaks of the asymmetric CH_3 bending bands move closer together in the latter, resulting in a single negative peak instead of a couplet. For each of the CH_3 bending vibrations, the vibrational couplings are small, so that only a single peak is observed.

4. Model Structure Setup

The only experimental ROA spectrum of a polypeptide that adopts a 3_{10}-helical conformation in solution has been reported in reference [49] for a specifically designed heptapeptide, labeled **7B** in the following discussion. Starting from the computational results obtained for 3_{10}-helical Ala_{20}, the ROA spectra of a series of polypeptides that provide a step-by-step model of the structural differences between Ala_{20} and **7B** was systematically investigated.

First, a shorter alanine polypeptide, Ala_{10}, with only ten amino acid residues is studied. Such a polypeptide is not long enough to support an α-helical conformation if the molecular structure is fully optimized and solvent effects are not explicitly included.[35,41] However, a regular 3_{10}-helix is the preferred conformation in such calculations because of the higher number of hydrogen bonds, so that ten amino acids are sufficient here. The backbone dihedral angles of the optimized Ala_{10} 3_{10}-helix are approximately $\phi = -62^\circ$ and $\psi = -19^\circ$; larger deviations occur only for the three residues at the O-terminal end. This backbone structure is identical to the one obtained for Ala_{20}. Therefore, all differences between the calculated ROA spectra of Ala_{20} and Ala_{10} can be attributed to the different chain lengths.

As a next step, the effect of a fourth substituent at the C^α atoms was investigated. For this purpose, a polypeptide composed of ten α-aminoisobutyric acid (Aib, see Scheme 1) residues, Aib_{10}, was investigated. In Aib, the C^α-hydrogen atom has been replaced by a methyl group, resulting in an achiral C^α-tetrasubstituted amino acid. For Aib_{10}, a right-handed, 3_{10}-helical conformation is considered, and backbone dihedral angles of approximately $\phi = -54^\circ$ and $\psi = -28^\circ$ were obtained for the optimized structure. Note, however, that because Aib is achiral, the right- and left-handed helical conformations are enantiomers. To achieve a preference for the right-handed 3_{10}-helical conformation, chiral amino acids have to be reintroduced. Thus, polypeptides built from isovaline (Iva) and α-methylnorvaline (α-Me-Nva) were investigated as the next step (see Scheme 1). Again, polypeptides with ten residues in a right-handed 3_{10}-helical conformation, which is now preferred over the left-handed form, were studied.

For Iva and α-Me-Nva, different side-chain conformations are possible. First, χ^1 (i.e. the N–C^α–C^β–C^γ dihedral angle) can adopt three different values. These conformations are illustrated in Scheme 2a and are referred to as *anti*-N ($\chi^1 \approx 180^\circ$), *anti*-CH_3 ($\chi^1 \approx +60^\circ$), and *anti*-CO ($\chi^1 \approx -60^\circ$). Second, for α-Me-Nva $\chi^{2,1}$ (i.e. the C^α–C^β–C^γ–C^δ dihedral angle, see Scheme 2b) could also be varied such that the *n*-propyl side chain was in either an *anti* ($\chi^{2,1} \approx 180^\circ$) or a *gauche* conformation ($\chi^{2,1} \approx \pm 60^\circ$). When calculating the ROA spectra of the Iva_{10} and (α-Me-Nva)$_{10}$ polypeptides, it is, however, not feasible to investigate all possible side-chain conformations. Therefore, only three different conformers were studied for each polypeptide, in which all residues adopt the *anti*-N, *anti*-CH_3, and *anti*-CO conformations, respectively, and for α-Me-Nva only the *anti* conformation of the *n*-propyl side chain was considered. The relative energies and structural parameters of the fully optimized structures are given in Table 1. For Iva_{10} and (α-Me-Nva)$_{10}$, the *all-anti*-N conformers are energetically preferred by 15.6 and 13.3 kJ mol^{-1}, respectively, compared with the *all-anti*-CH_3 structures. It can, therefore, be estimated that the energies of conformers in which only one side chain adopts a different conformation are about 2 kJ mol^{-1} above the most stable conformation and such conformers are populated at room temperature and contribute to the observed ROA spectra. For all optimized structures of Iva_{10} and (α-Me-Nva)$_{10}$, the backbone dihedral angles differ from those obtained for Aib_{10} by no more than 5°. The fully optimized molecular structures of all investigated polypeptides are shown in the Supporting Information.

Finally, the polypeptide **7B** is considered, which is an α-Me-Nva heptapeptide, in which two residues have been replaced

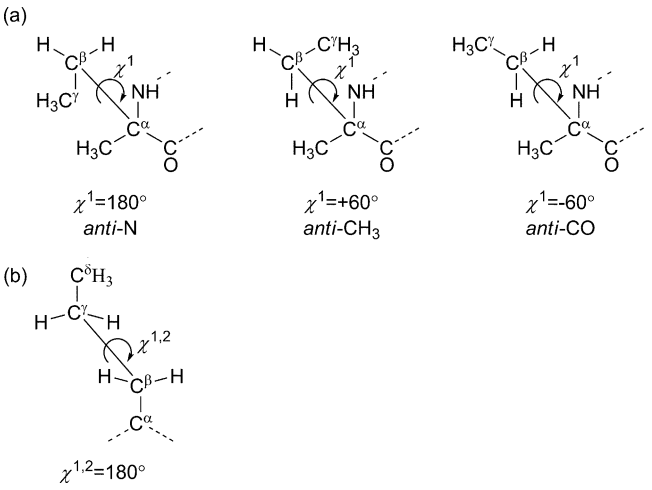

Scheme 2. Different possible side-chain conformations for Iva and α-Me-Nva.

Table 1. Approximate backbone and side chain dihedral angles in the optimized structures of the investigated polypeptides. For Iva_{10} and (α-Me-Nva)$_{10}$, the relative energies, E_{rel}, of the considered conformers are also given.

		ϕ [°]	ψ [°]	χ^1 [°]	$\chi^{2,1}$ [°]	E_{rel} [kJ mol^{-1}]
Ala_{20}		−63	−19			
Ala_{10}		−62	−19			
Aib_{10}		−54	−28			
Iva_{10}	*anti*-N	−52	−30	180		0.0
	anti-CH_3	−58	−23	+60		15.6
	anti-CO	−55	−28	−60		22.5
(α-Me-Nva)$_{10}$	*anti*-N	−51	−31	180	180	0.0
	anti-CH_3	−57	−23	+60	180	13.3
	anti-CO	−55	−29	−60	180	19.8
7B		−50/−63	−32/−16	180	180	

by 2-amino-3-[1-(1,4,7-triazacyclononane)]-L-propanoic acid (L-ATANP, see Scheme 1) units and which has been terminated with methoxy and acetyl groups. Here, only the most stable conformation for the side chains is considered (i.e. the *anti*-N conformation for χ^1 in α-Me-Nva as well as ATANP and the *anti*-conformation for the *n*-propyl side chains of α-Me-Nva). In addition, several conformations are possible for the TAN rings, which were not systematically investigated. Since **7B** contains both C^α-trisubstituted and C^α-tetrasubstituted amino acids, the backbone dihedral angles in the optimized structure (shown in Figure 2) vary between those of Ala_{10} and of Aib_{10}.

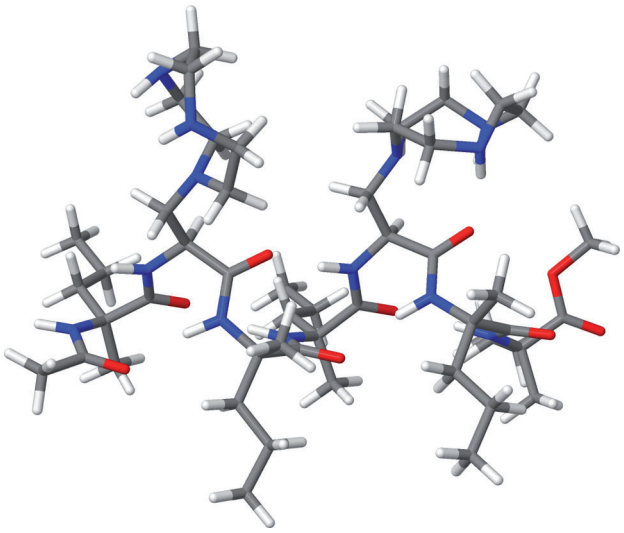

Figure 2. Optimized molecular structure of the 3_{10}-helical model heptapeptide **7B**.

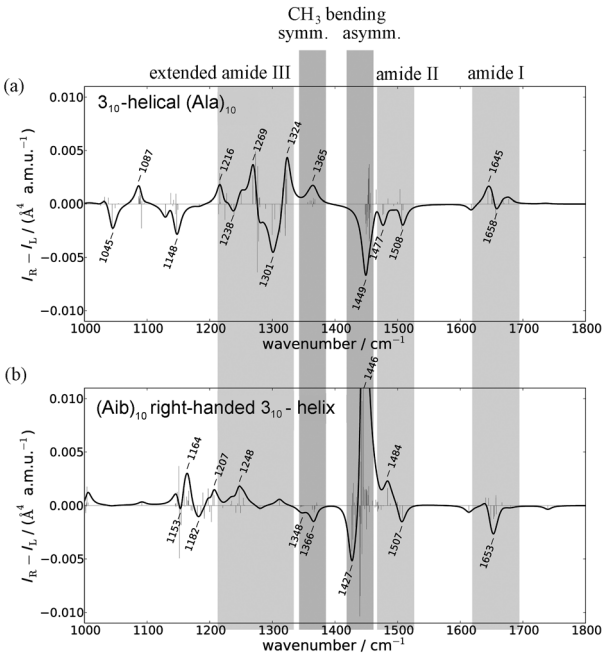

Figure 3. Calculated ROA spectra of a) 3_{10}-helical $(Ala)_{10}$ and b) 3_{10}-helical $(Aib)_{10}$ in the right-handed conformation. The spectra have been plotted by using a Lorentzian line width of 15 cm^{-1} and the individual transitions have been included as a line spectrum scaled by 0.04.

5. Analysis of the ROA Spectra of 3_{10}-Helical Polypeptides

5.1. Chain Length: $(Ala)_{20}$ versus $(Ala)_{10}$

A comparison of the calculated ROA spectra of Ala_{20} (shown in Figure 1a) and of Ala_{10} (shown in Figure 3a) makes it possible to assess the effect of the shorter peptide chain on the ROA spectra. Overall, there is good agreement between the spectra. For the CH_3 bending vibrations, as well as for the C^α–N and C–C stretching region, the positions of the ROA bands are unchanged. Their intensities and band shapes also remain qualitatively similar, but there are slight changes in their relative intensities. Except for some differences in the amide III band, the spectra also agree for the extended amide III region. For the amide II band, the shape with two negative peaks is not affected, but both amide II peaks shift by about 8 cm^{-1} to lower wavenumbers. For all bands in Ala_{10}, the localized modes obtained for residues in the center of the helix, which are shown in the Supporting Information, are identical to those of Ala_{20} (see Figure 1b).

The only major difference between the ROA spectra of Ala_{20} and Ala_{10} occurs for the amide I band. The couplet (positive at lower wavenumbers and negative at higher wavenumbers) for Ala_{20} disappears and is replaced by a positive peak, which is also shifted to higher wavenumbers. This change in the amide I band can be investigated by considering the corresponding localized modes. The wavenumbers and the ROA intensities of one localized mode from the center of the helices are compared in Table 2. The wavenumber of this mode shifts to higher wavenumbers, which corresponds to the shift of the

Table 2. Wavenumbers, $\tilde{\nu}$ (in cm^{-1}) and ROA intensities (int.; in 10^{-3} $Å^4$/a.m.u.) for representative localized modes obtained for the amide I, II, and III bands in 3_{10}-helical polypeptides. For Ala_{20}, the localized modes on the peptide link between residues 9 and 10 are considered, for all other polypeptides those on the peptide link between residues 5 and 6.

		Amide I		Amide II		Amide III	
		$\tilde{\nu}$	int.	$\tilde{\nu}$	int.	$\tilde{\nu}$	int.
Ala_{20}		1640	1.5	1502	−9.4	1242	10.5
Ala_{10}		1652	6.0	1494	−9.7	1235	−1.6
Aib_{10}		1650	−6.5	1496	−3.3	1249	6.8
Iva_{10}	*anti*-N	1643	−4.3	1499	3.9	1237	−4.9
	anti-CH_3	1642	−10.6	1494	10.4	1227	6.0
	anti-CO	1645	−4.0	1490	−2.8	1239	13.6
$(α\text{-Me-Nva})_{10}$	*anti*-N	1643	−1.6	1499	2.5	1227	0.9
	anti-CH_3	1643	−8.3	1493	15.6	1221	8.8
	anti-CO	1643	−1.9	1489	7.5	1237	15.2

amide I band. However, while for Ala_{20} the wavenumbers and ROA intensities of the localized modes in the center of the helix agree with each other and deviations occur only for the modes on the terminal residues, these deviations are much more significant for the shorter Ala_{10} helix. A list of all amide I localized modes for Ala_{20} and Ala_{10} is given in the Supporting Information. For Ala_{10}, the wavenumbers of the localized modes on the two residues at each end of the helix are about 10 cm^{-1} higher than those of the modes from the center of the helix. In addition, the ROA intensities of these terminal modes are significantly higher. For the shorter helix, these end-group effects alter the amide I band in the final ROA spectra more significantly.

The amide I couplet in 3_{10}-helical Ala_{20}, which is opposite to the one in the corresponding α helix, could be traced back to the vibrational coupling constants and the observation that the negative second-nearest-neighbor coupling is the largest in magnitude (see Table 3). This pattern is preserved for Ala_{10}. The magnitude of the first- and second-nearest-neighbor coupling constants decreases, but the second-nearest-neighbor coupling of -3.3 cm^{-1} still dominates, compared to a nearest-neighbor coupling of $+2.4$ cm^{-1}. The intensity coupling matrices for Ala_{10} and Ala_{20} remain qualitatively unchanged, even though the nearest-neighbor intensity coupling decreases (see Supporting Information). Hence, one should still observe an amide I couplet that is positive at lower wavenumbers and negative at higher wavenumbers in Ala_{10}. However, because of the shorter chain length, the splitting between the positive and the negative parts is significantly reduced. Moreover, the localized modes on the terminal residues interfere with this couplet, so that in the final ROA spectrum, the amide I band is dominated by a single positive peak. Finally, note that the vibrational couplings constants (see Table 3 and Supporting Information, respectively) and the intensity coupling constants (see Supporting Information) do not change significantly for the amide II and III bands.

Table 3. Vibrational coupling constants (in cm^{-1}) obtained for the amide I and II bands in 3_{10}-helical polypeptides. For Ala_{20}, the coupling constants refer to the coupling between the localized modes on the peptide link between residues 7 and 8 and those on subsequent ones. For all other polypeptides the coupling between the localized modes on the peptide link between residues 4 and 5 and its neighbors is given.

		Amide I				Amide II			
		1st	2nd	3rd	4th	1st	2nd	3rd	4th
Ala_{20}		+2.7	−3.7	−0.8	−0.6	−6.2	−3.5	+1.1	−0.3
Ala_{10}		+2.4	−3.3	−0.3	−0.7	−5.8	−3.4	+1.1	−0.2
Aib_{10}		+2.9	−3.0	−0.5	−0.5	−4.2	−2.7	+1.2	−0.1
Iva_{10}	*anti*-N	+2.9	−3.4	−0.6	−0.4	−4.1	−2.3	+1.0	−0.1
	anti-CH_3	+2.8	−2.7	−0.4	−0.5	−3.7	−2.1	+1.0	0.0
	anti-CO	+2.8	−3.0	−0.4	−0.4	−4.8	−2.3	+0.8	−0.1
(α-Me-Nva)$_{10}$	*anti*-N	+3.0	−3.3	−0.6	−0.5	−4.1	−2.3	+1.0	−0.1
	anti-CH_3	+2.6	−2.6	−0.1	−0.5	−3.7	−2.6	+0.9	−0.1
	anti-CO	+2.8	−2.9	−0.4	−0.3	−5.3	−2.5	+1.0	−0.2

5.2. C^{α}-Substitution Pattern: $(Ala)_{10}$ versus $(Aib)_{10}$

Next, the effect of C^{α}-tetrasubstitution on the ROA spectra can be investigated by comparing the calculated spectra of Ala_{10} and Aib_{10}, in which the hydrogen atoms at the C^{α} atom are replaced by methyl groups. Both spectra are shown in Figure 3. It is important to note that Aib is an achiral amino acid. Therefore, the ROA spectrum of Aib_{10} is solely due to the global chirality of the helical structure,[35] and there is no contribution of the local chirality of the amino acids.

The ROA spectrum of Aib_{10} differs significantly from that of Ala_{10}. For the amide I band, one now finds a negative peak. This sign change is reflected by the ROA intensities of the localized modes on the central residues (see Table 2). Nevertheless, the pattern found for the vibrational coupling constants (see Table 3) is still the same as for the 3_{10}-helical alanine polypeptides, with a positive nearest-neighbor coupling and a negative second-nearest coupling constant, which is larger in magnitude. However, the nearest-neighbor coupling increases and as a result the difference in magnitude between the first and second nearest-neighbor coupling becomes very small. For the amide II band, the sign of the localized mode ROA intensities (see Table 2) changes from negative to positive. Moreover, instead of two negative peaks, one now finds a couplet that is negative at lower wavenumbers and positive at higher wavenumbers. While the amide II vibrational coupling constants are similar for Ala_{10} and Aib_{10}, this different band shape can be related to the increase of the nearest-neighbor intensity coupling terms (see the Supporting Information).

In the extended amide III region, large qualitative changes appear. Whereas there are three bands in this region for the alanine polypeptides (the amide III band as well as two C^{α}–H bending bands), there is only one band for Aib_{10}. The representative localized modes for the bands in this region are shown in Figure 4. Because there are no C^{α}-hydrogen atoms in Aib_{10}, the corresponding C^{α}–H bending bands disappear and only the amide III band remains. The amide III localized mode also differs. For the alanine polypeptides, the classical amide III vibration couples with the C^{α}–H bending vibrations, and the resulting amide III localized modes are combinations of these vibrations. Because of this coupling, its ROA intensity is due to the vibrational chirality resulting from the chiral arrangement of the peptide group and the C^{α}–H group. In contrast, for Aib_{10}, the amide III band is only due to the classical amide III vibration. Since the peptide group is not chiral by itself, its ROA intensity is, in this case, only determined by the electronic chirality of the helical structure. Hence, the extended amide III region can be expected to be much less sensitive to structural

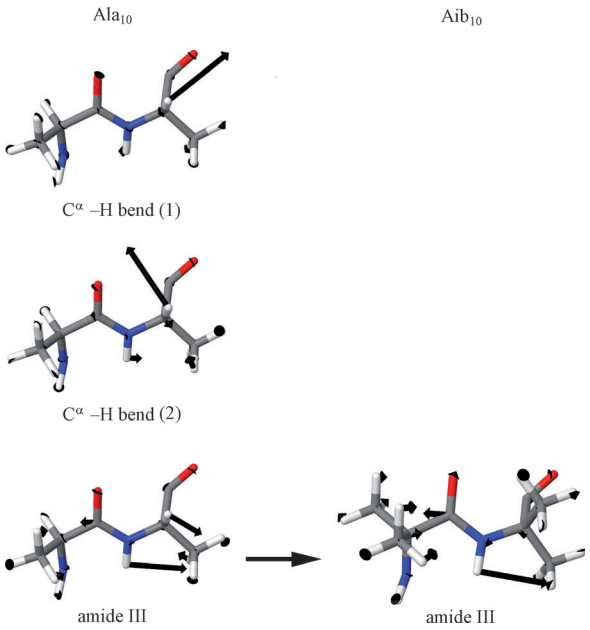

Figure 4. Representative localized modes corresponding to the extended amide III region in Ala_{10} (left) and in Aib_{10} (right). The localized modes on the peptide link between residues 5 and 6 have been chosen here. Only those atoms that contribute significantly are shown.

changes in Aib polypeptides because coupling between classical amide III vibration and C^{α}–H vibrations is not present. Finally, the absence of this coupling also leads to a shift of the amide III band to higher wavenumbers (see Table 2).

Differences between Ala_{10} and Aib_{10} are also observed for the asymmetric CH_3 bending band, for which a strong couplet is found instead of a negative peak, and for the symmetric CH_3 bending band, which changes its sign. These bands are discussed in the following section. Finally, note that large changes are also observed in the C^{α}–N and C–C stretching region below 1200 cm^{-1}. This is due to the additional C^{α}–C^{β} stretching vibration in Aib_{10}, which mixes with the other vibrations in this region.

5.3. Variation of Side Chains and Side-Chain Conformation: Iva_{10} and $(\alpha\text{-Me-Nva})_{10}$

As a further step, the polypeptides Iva_{10} and $(\alpha\text{-Me-Nva})_{10}$, which are composed of chiral C^{α}-tetrasubstituted amino acids with larger aliphatic side chains, are investigated. Thus, in addition to the global chirality of the right-handed helical structure, the local chirality of the amino acid building blocks is reintroduced. The calculated ROA spectra for the three conformers considered for Iva_{10} and $(\alpha\text{-Me-Nva})_{10}$ are shown in Figure 5, with the spectra of the most stable *anti*-N conformers given on top.

For both Iva_{10} and $(\alpha\text{-Me-Nva})_{10}$, the three amide bands are rather small for all conformers. The corresponding localized modes, which are shown in the Supporting Information, are similar to those obtained for Aib_{10} in all cases. The amide I band features a negative peak or a weak couplet at approximately the same position as that in Aib_{10}. In line with the negative total intensity of the amide I band, the ROA intensity of the localized modes on the central residues is also negative for all conformers (see Table 2). However, relative to Aib_{10}, these localized modes are shifted to lower wavenumbers by about 7 cm^{-1}. But as discussed earlier for Ala_{10}, large deviations are observed for the localized modes on the terminal residues, which are shifted to higher wavenumbers and exhibit a positive ROA intensity. These end-group effects significantly alter the position and shape of the amide I ROA band. For the vibrational coupling constants, which are compared in Table 3, the pattern found for the alanine polypeptides and for Aib_{10} is preserved. The nearest-neighbor coupling is positive, whereas the second-nearest-neighbor coupling is negative. In addition, for most of the conformers the second-nearest-neighbor coupling is larger in magnitude. However, the magnitudes of the first and the second-nearest-neighbor couplings approach each other. Consequently, the resulting splitting between the normal modes is small and instead of a couplet only a single negative peak is found for most conformers.

For the amide II band, the localized modes show the same wavenumbers as those of Aib_{10} and the ROA intensity is still rather small, even though its sign changes. In addition, the vibrational coupling constants (see Table 3) are similar, resulting in a couplet. At lower wavenumbers this couplet partly overlaps with the adjacent CH_3 bending bands. The representative localized modes obtained for the amide III band (see Table 2) are shifted to lower wavenumbers than those of Aib_{10} and have a small and, for most conformers, positive ROA intensity. In contrast to the alanine polypeptides and also to Aib_{10}, the vibrational coupling constants of the amide III band (see the Supporting Information) become very small. As a result, only a single peak is observed in the calculated ROA spectra.

The strongest signals in the ROA spectra of Iva_{10} and $(\alpha\text{-Me-Nva})_{10}$ appear in the region between about 1250 and 1470 cm^{-1}. This region includes vibrations of the side chain CH_3 and CH_2 groups and, therefore, also shows the biggest changes upon introduction of larger aliphatic side chains and variation of the side-chain conformation. To start, the region between about 1420 and 1470 cm^{-1}, which is labeled as the asymmetric CH_3 bending region in Figure 5, is considered. Representative localized modes obtained for the bands in this region for the different 3_{10}-helical polypeptides are shown in Figure 6, and the wavenumbers and ROA intensities of these localized modes are summarized in Table 4.

For the alanine polypeptides, this region contains the two almost degenerate asymmetric CH_3 bending vibrations at about 1450 cm^{-1}. While one of these modes has a positive and the other one has a negative ROA intensity, they are not separated in the ROA spectrum and a single negative ROA band shows up in the calculated spectra. For Aib_{10}, an additional methyl group is introduced and consequently there are four almost degenerate asymmetric CH_3 bending vibrations at around 1450 cm^{-1}. The localized modes all have positive ROA intensities. However, the vibrations on the two methyl groups couple with each other and form one negative ROA band at 1427 cm^{-1} and a stronger positive band at 1446 cm^{-1}.

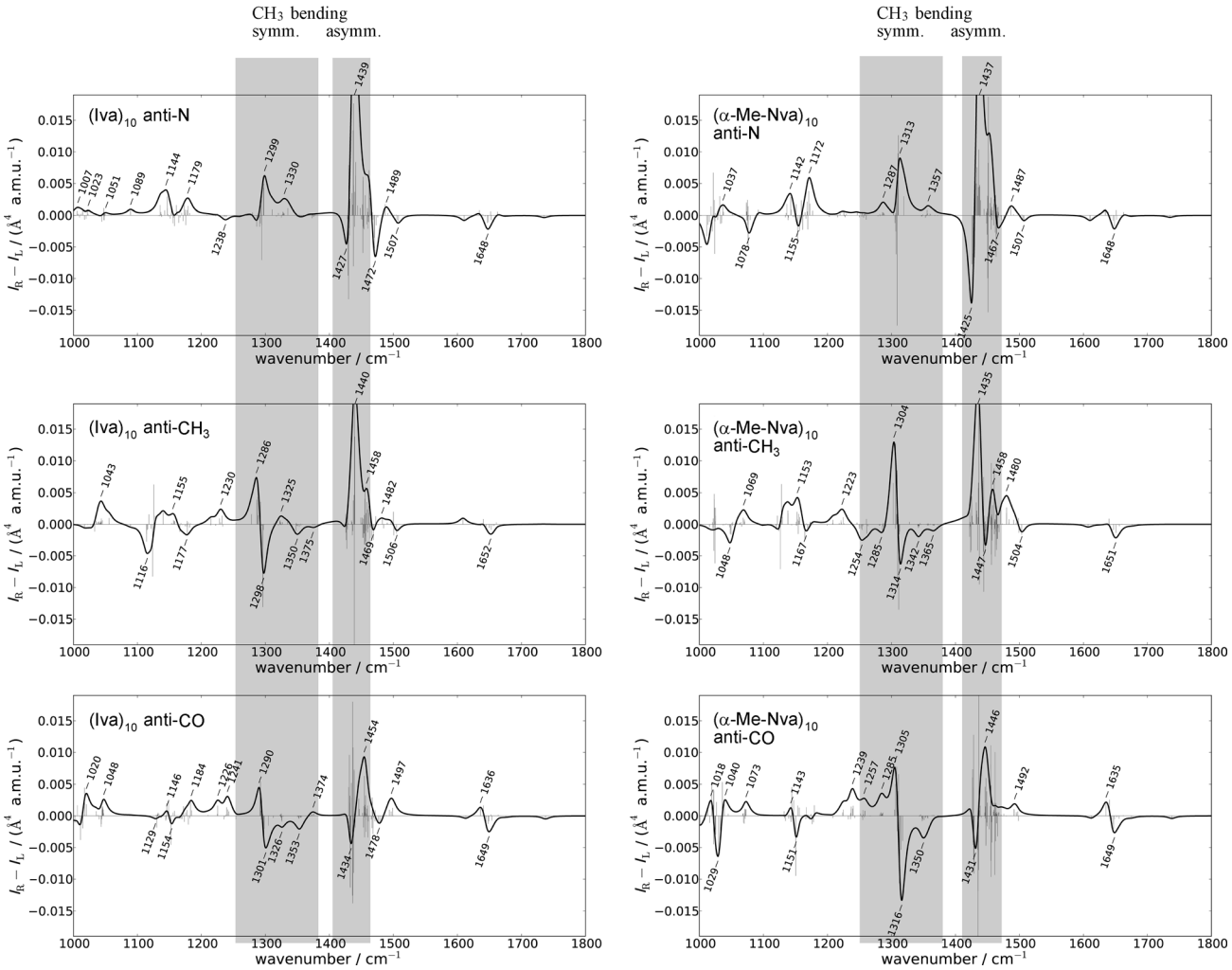

Figure 5. Calculated ROA spectra the three considered conformers of Iva_{10} (left) and (α-Me-Nva)$_{10}$ (right). The spectra have been plotted by using a Lorentzian line width of 15 cm^{-1} and the individual transitions have been included as a line spectrum scaled by 0.04.

For Iva_{10}, the two methyl groups ($C^{\beta}H_3$ and $C^{\gamma}H_3$) become inequivalent and, in addition, a $C^{\beta}H_2$ group is introduced. For the band at 1450–1470 cm^{-1}, three localized modes are obtained on each residue. These correspond to one of the asymmetric $C^{\beta}H_3$ bending vibrations and the two asymmetric $C^{\gamma}H_3$ bending vibrations. The second asymmetric $C^{\beta}H_3$ bending vibration combines with the scissoring vibration of the $C^{\beta}H_2$ group, resulting in two localized modes at about 1437 and 1430 cm^{-1}. For the *anti*-N conformation, the three asymmetric CH_3 bending localized modes have in total a negative ROA intensity, which results in a negative peak at 1472 cm^{-1}. The localized modes for the higher wavenumber combination of asymmetric $C^{\beta}H_3$ bending and $C^{\beta}H_2$ scissoring have a large positive ROA intensity, leading to a very strong positive peak at 1439 cm^{-1}. For the lower wavenumber combination, the localized modes have a large negative ROA intensity, which gives rise to a negative peak at 1427 cm^{-1}. For the *anti*-CH_3 conformation, the relative intensities of the different localized modes and the peaks in the final ROA spectrum differ, but the overall pattern is still similar. On the other hand, for the *anti*-CO conformer, the ROA intensity of the three asymmetric CH_3 bending localized modes becomes positive, whereas the intensity of both CH_2 scissoring localized modes becomes negative, resulting in a shift of the strong positive peak in the ROA spectrum to higher wavenumbers. Nevertheless, for all three conformers the region between about 1420 and 1470 cm^{-1} is dominated by a strong positive peak (either at 1440 cm^{-1} for the *anti*-N and *anti*-CH_3 conformations or shifted to 1454 cm^{-1} for the *anti*-CO conformation), with an adjacent negative feature at the lower wavenumber end at about 1430 cm^{-1}. This negative peak is strongest for the *anti*-CO conformation and almost disappears for the *anti*-CH_3 conformer.

For (α-Me-Nva)$_{10}$, a second CH_2 group is introduced. The scissoring vibration of this additional $C^{\gamma}H_2$ unit combines with one of the asymmetric $C^{\delta}H_3$ vibrations. Hence, there are four localized modes with wavenumbers between 1445 and 1470 cm^{-1}: one asymmetric $C^{\beta}H_3$ bending vibration, one asymmetric $C^{\gamma}H_3$ bending vibration, and two combinations of the other asymmetric $C^{\gamma}H_3$ bending vibration with the $C^{\gamma}H_2$ scissoring vibration. The two combinations of the other asymmetric $C^{\beta}H_3$ bending vibration with the $C^{\beta}H_2$ scissoring vibration appear at about 1435 and 1425–1430 cm^{-1}, that is, at slightly

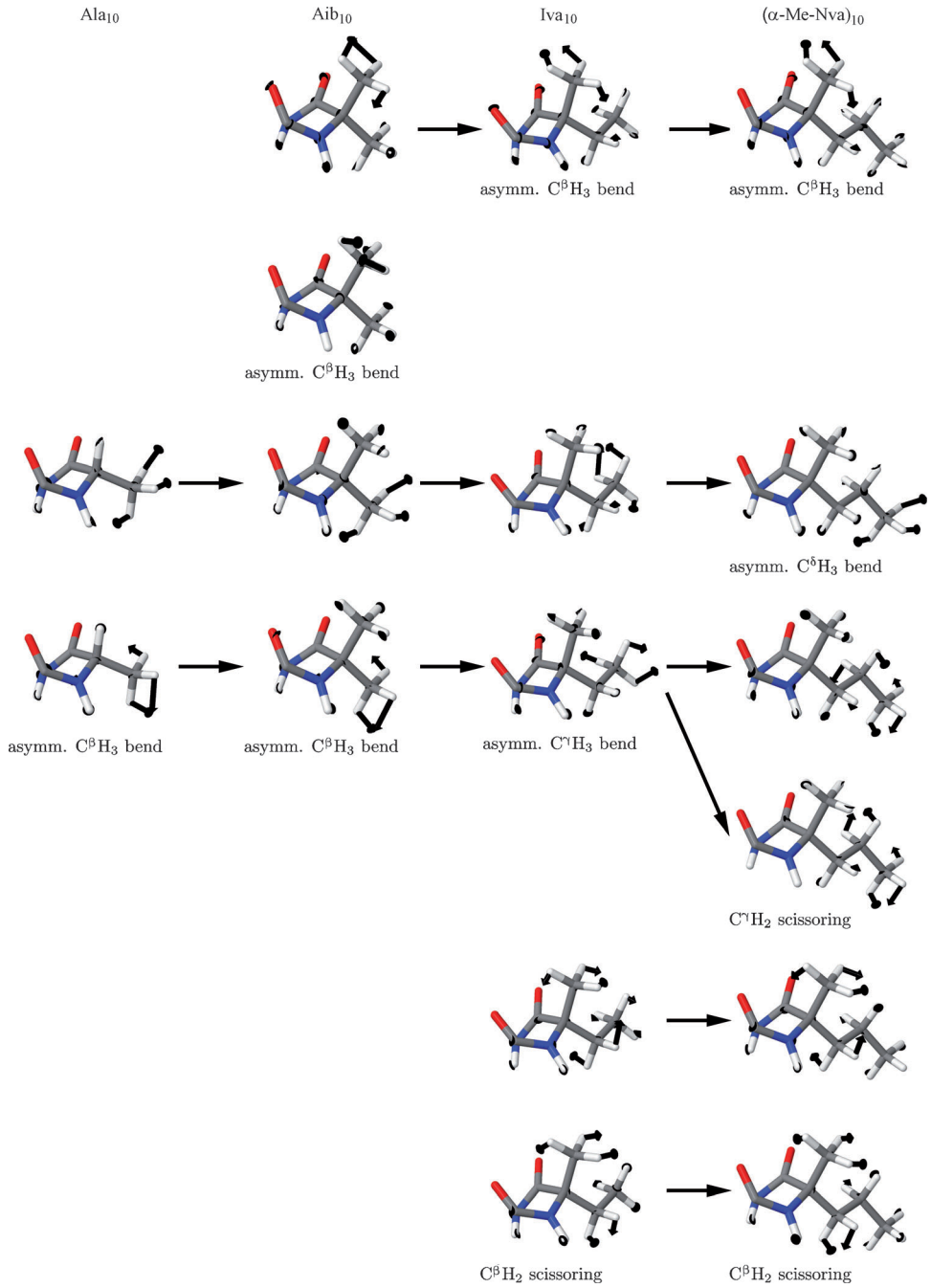

Figure 6. Representative localized modes for the bands in the asymmetric CH_3 region in Ala_{10}, Aib_{10}, Iva_{10}, and $(\alpha\text{-Me-Nva})_{10}$. For Iva_{10} and $(\alpha\text{-Me-Nva})_{10}$, the *anti*-N conformer is considered, but similar localized modes are also obtained for the other conformers. The localized modes on residue 6 have been chosen here. Only those atoms that contribute significantly are shown.

lower wavenumbers than those in Iva_{10}. The ROA intensities of the localized modes qualitatively agree with those of Iva_{10}. For the *anti*-N and *anti*-CH_3 conformers, the four localized modes between 1445 and 1470 cm^{-1} have a negative ROA intensity in total, which gives rise to negative features at 1467 and 1447 cm^{-1}, respectively, whereas the $C^{\beta}H_2$ scissoring vibrations yield a very strong positive peak at about 1435 cm^{-1} and for the *anti*-N conformer a negative peak at 1425 cm^{-1}, which disappears for the *anti*-CH_3 conformation. As for Iva_{10}, in the *anti*-CO conformer the ROA intensity of the localized modes at higher wavenumbers increases, resulting in a shift of the strong positive ROA peak. Altogether, in the 1420–1470 cm^{-1} region the resulting ROA spectra of Iva_{10} and $(\alpha\text{-Me-Nva})_{10}$ are in good agreement with each other for each of the three considered conformers.

Finally, ROA signals due to the aliphatic amino acid side chains also appear in the region between about 1260 and 1380 cm^{-1}. This region is labeled as the symmetric CH_3 bending region in Figure 5. For the considered 3_{10}-helical polypeptides, the corresponding localized modes for each band in this region are shown in Figure 7, and the wavenumbers and ROA intensities of these localized modes are compared in Table 5.

For the alanine polypeptides, there is only the symmetric $C^{\beta}H_3$ bending vibration at around 1366 cm^{-1} in this region, with a small positive ROA intensity. For Aib_{10}, the additional methyl group introduces a second symmetric $C^{\beta}H_3$ bending vibration at 1351 cm^{-1}. Both symmetric $C^{\beta}H_3$ bending vibrations still have a rather small ROA intensity that changes its sign and becomes negative when going from Ala_{10} to Aib_{10}. In Iva_{10}, the two methyl groups become inequivalent and the symmetric $C^{\gamma}H_3$ bending vibration shifts up to 1370–1376 cm^{-1}, whereas the symmetric $C^{\beta}H_3$ bending vibration stays at about 1350 cm^{-1}. In addition, two vibrations of the $C^{\beta}H_2$ group appear in the considered region: the wagging vibration at about 1325 cm^{-1} and the twisting vibration at about 1295 cm^{-1}. Finally, for $(\alpha\text{-Me-Nva})_{10}$, the position of the symmetric $C^{\delta}H_3$ bending vibration moves slightly to 1365–1370 cm^{-1}. In addition, because of the second CH_2 group, there are now two CH_2 wagging and two CH_2 twisting vibrations. These two wagging and twisting vibrations each couple and form an in-phase and an out-of-phase combination. For the wagging vibrations, the out-of-phase combination again couples with the symmetric $C^{\beta}H_3$ bending vibration, resulting in two localized modes at

Table 4. Wavenumbers, $\tilde{\nu}$ (in cm^{-1}), and ROA intensities (in 10^{-3} Å^4/a.m.u.) for representative localized modes obtained for the bands in the asymmetric CH_3 bending region in 3_{10}-helical polypeptides. For Ala_{20}, the localized modes on residue 10 are considered; for all other polypeptides those on residues 6.

		Asymm. $C^\beta H_3$		Asymm. $C^{\gamma\delta}H_3$		$C^\gamma H_2$ scissor.		$C^\beta H_2$ scissor.	
		$\tilde{\nu}$	int.	$\tilde{\nu}$	int.	$\tilde{\nu}$	int.	$\tilde{\nu}$	int.
Ala_{20}		1452	−10.3						
		1452	12.8						
Ala_{10}		1454	−13.5						
		1452	6.2						
Aib_{10}		1450	2.8						
		1446	19.7						
		1450	6.5						
		1445	8.4						
Iva_{10}	*anti*-N	1465	−11.7	1463	9.8			1437	134.0
		–[a]		1455	−7.8			1431	−81.5
	anti-CH_3	1464	0.2	1456	-0.1			1438	49.3
		–[a]		1455	−19.5			1427	−3.2
	anti-CO	1463	1.5	1459	17.5			1437	−26.4
		–[a]		1457	21.7			1433	−70.9
(α-Me-Nva)$_{10}$	*anti*-N	1463	−13.9	1456	−3.0	1466	5.5	1438	113.9
		–[a]		–[b]		1451	0.4	1430	−54.5
	anti-CH_3	1463	−4.8	1457	8.2	1462	15.6	1433	85.2
		–[a]		–[b]		1445	−59.7	1424	−10.0
	anti-CO	1463	−1.8	1456	2.8	1462	−17.1	1437	−6.9
		–[a]		–[b]		1448	16.4	1429	5.7

[a] The second asymmetric $C^\beta H_3$ bending vibration combines with the $C^\beta H_2$ scissoring vibration. [b] The second asymmetric $C^\delta H_3$ bending vibration combines with the $C^\gamma H_2$ scissoring vibration.

Table 5. Wavenumbers, $\tilde{\nu}$ (in cm^{-1}), and ROA intensities (in 10^{-3} Å^4/a.m.u.) for representative localized modes obtained for the bands in the symmetric CH_3 bending region in 3_{10}-helical polypeptides. For Ala_{20}, the localized modes on residue 10 are considered; for all other polypeptides those on residues 6. For the CH_2 wagging and twisting vibrations in (α-Me-Nva)$_{10}$, the out-of-phase combinations are labeled "(o)", whereas "(i)" is used to label the in-phase combinations.

		Symm. $C^{\gamma\delta}H_3$		Symm. $C^\beta H_3$		CH_2 wagging			CH_2 twisting		
		$\tilde{\nu}$	int.	$\tilde{\nu}$	int.	$\tilde{\nu}$		int.	$\tilde{\nu}$		int.
Ala_{20}				1368	4.2						
Ala_{10}				1366	4.9						
Aib_{10}				1363	−2.6						
				1351	−3.9						
Iva_{10}	*anti*-N	1375	−0.3	1353	−2.0		1327	5.1		1293	14.2
	anti-CH_3	1376	−1.3	1350	−6.5		1324	4.8		1294	3.7
	anti-CO	1370	1.6	1352	−4.8		1325	−5.0		1296	0.8
(α-Me-Nva)$_{10}$	*anti*-N	1368	+0.2	–[a]		(o)	1356	2.4	(i)	1309	18.5
						(o)	1348	−0.7	(o)	1259	−2.0
						(i)	1286	4.1			
	anti-CH_3	1366	−3.3	–[a]		(o)	1357	2.1	(i)	1308	18.7
						(o)	1342	−6.7	(o)	1259	−5.9
						(i)	1288	−9.3			
	anti-CO	1365	1.7	–[a]		(o)	1353	−5.9	(i)	1312	−10.4
						(o)	1347	−6.9	(o)	1257	7.5
						(i)	1286	7.9			

[a] For (α-Me-Nva)$_{10}$, the symmetric $C^\beta H_3$ bending vibration combines with the out-of-phase CH_2 wagging vibration.

1345 and at 1355 cm^{-1}, whereas the in-phase wagging localized mode appears at 1285–1290 cm^{-1}. For the twisting vibrations, the in-phase combination shows up at 1310 cm^{-1}, whereas the out-of-phase combination appears at 1260 cm^{-1}.

For all bands in the symmetric CH_3 bending region between about 1260 and 1380 cm^{-1}, the ROA intensities of the corresponding localized modes (see Table 5), and thus, the total intensities of the resulting bands in the ROA spectrum are also rather small. The only exception is the CH_2 twisting vibration in the *anti*-N conformation of Iva_{10} and the in-phase CH_2 twisting vibration in all three conformers of (α-Me-Nva)$_{10}$. In the spectra of the *anti*-N conformers of Iva_{10} and (α-Me-Nva)$_{10}$, this vibration shows up as positive ROA signals at 1299 and 1313 cm^{-1}, respectively.

The vibrational coupling constants and the intensity coupling matrices for the bands in the symmetric CH_3 bending region are included in the Supporting Information. For all bands, the vibrational coupling constants are rather small; the largest are found for the CH_2 twisting bands, where the nearest-neighbor coupling is between −0.7 and 3.0 cm^{-1}. For most bands, the intensity coupling terms are also small and as a result the ROA spectra show very weak signals. The only exception is the CH_2 twisting vibration in Iva_{10} and the in-phase CH_2 twisting vibration in (α-Me-Nva)$_{10}$, for which very large intensity coupling terms are obtained. For the *anti*-N conformers, the nearest-neighbor intensity couplings are negative; therefore, a strong couplet that is negative at low wavenumbers and positive at high wavenumbers should result. However, the positive and negative parts of this couplet are very close, so that they overlap and the resulting ROA spectra only show a single positive peak. For the *anti*-CH_3 and *anti*-CO conformers, the nearest-neighbor intensity coupling is positive. Therefore, the corresponding CH_2 twisting and in-phase CH_2 twisting bands show a very strong couplet that is positive at low wavenumbers and negative at higher wavenumbers. Note that the intensity coupling terms are determined by the orientation of the localized modes with respect to each other. Therefore, the very large intensity couplings found for the CH_2 twisting and in-phase CH_2

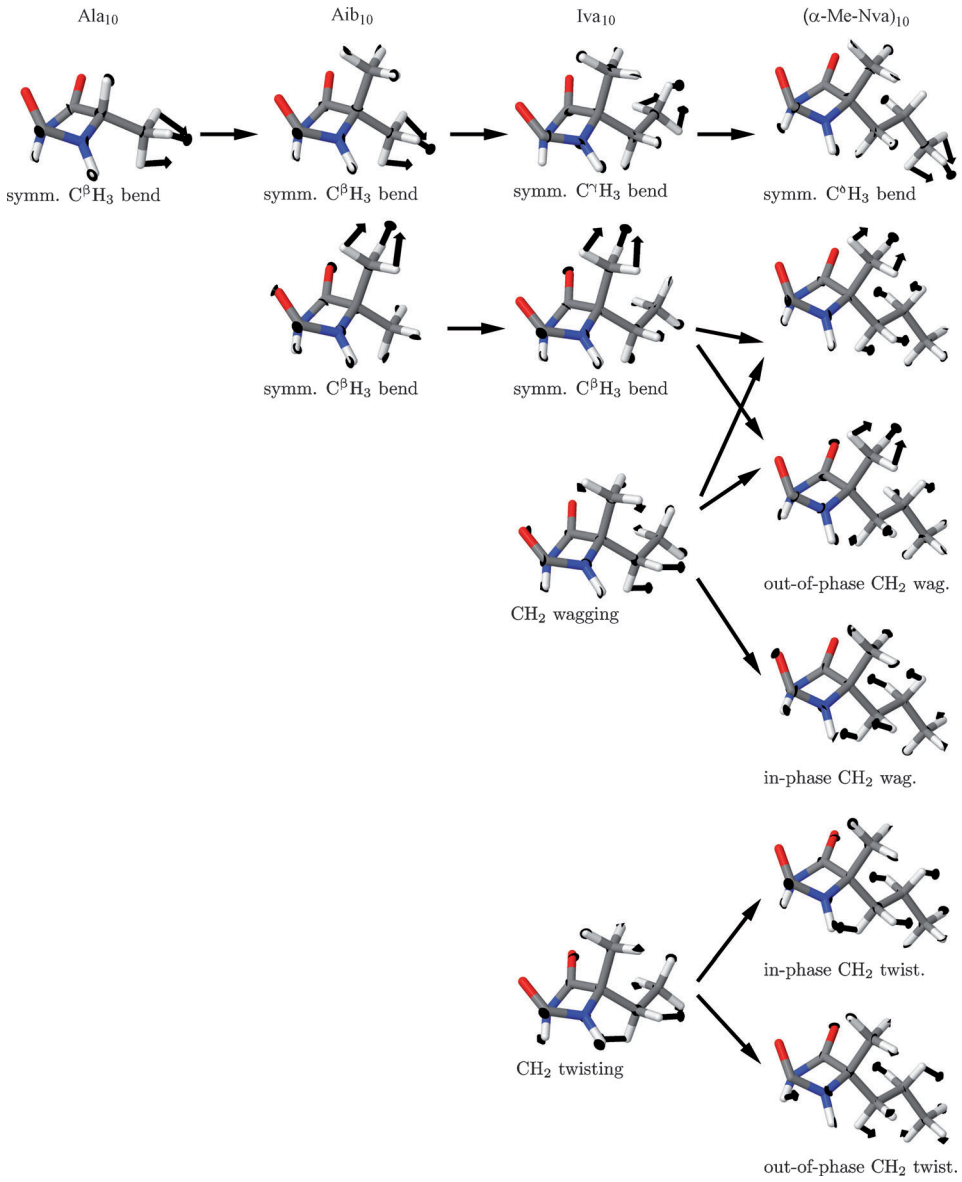

Figure 7. Representative localized modes for the bands in the symmetric CH_3 region in Ala_{10}, Aib_{10}, Iva_{10}, and $(\alpha\text{-Me-Nva})_{10}$. For Iva_{10} and $(\alpha\text{-Me-Nva})_{10}$, the *anti*-N conformer is considered, but similar localized modes are also obtained for the other conformers. The localized modes on residue 6 have been chosen here. Only those atoms that contribute significantly are shown.

twisting bands are directly related to the specific helical structure.

6. Comparison with Experimental Spectra

A comparison with the experimental ROA spectrum of 3_{10}-helical **7B** is now possible. The calculated ROA spectrum of this heptapeptide of α-Me-Nva, which contains two L-ATANP units, is shown on the left-hand side of Figure 8a. For **7B**, only the most stable *anti*-N conformation of the α-Me-Nva side chains and only one conformation of the TAN rings in the L-ATANP side chains were considered. Because of the structural similarity, the calculated ROA spectrum largely agrees with that of the *anti*-N conformer of $(\alpha\text{-Me-Nva})_{10}$. The three amide bands are rather small, the asymmetric CH_3 bending region is dominated by a large couplet that is positive at 1435 cm^{-1} and negative at 1426 cm^{-1}, and there is a strong positive signal at 1300–1310 cm^{-1} in the symmetric CH_3 bending region.

However, there are also several significant differences between the calculated ROA spectra of the *anti*-N conformer of $(\alpha\text{-Me-Nva})_{10}$ and the considered conformer of **7B**. First, the couplet in the asymmetric CH_3 bending region at 1435/1426 cm^{-1} is smaller, which can be attributed to the shorter chain lengths of **7B**. Second, there is an additional strong negative peak at 1354 cm^{-1} and, third, the peak in the symmetric CH_3 bending region at 1300–1310 cm^{-1} is broader and shows two distinct maxima.

These differences can mainly be attributed to vibrations of the TAN rings. Therefore, these features can be expected to be sensitive to the ring conformations and a reliable prediction would require careful sampling of the different ring conformations in combination with suitable averaging of the corresponding ROA spectra. While this can be achieved for small molecules, such as single amino acids[66,67] or carbohydrates,[68] this is currently not feasible for the polypeptides considered herein. To estimate how these ring vibrations alter the ROA spectrum of **7B**, contributions of the TAN rings to the ROA intensities can be removed by setting the property tensor derivatives for the atoms in these rings to zero. This is motivated by the previous observation by Bouř and co-workers that averaging over the low-frequency vibrations of flexible rings can lead to a cancellation of the corresponding ROA signals.[67] The ROA spectrum without the contributions of the TAN rings is shown in Figure 8b (left). It turns out that the positive peak at 1484 cm^{-1} and the negative peak at 1354 cm^{-1} disappear, that is, these features are indeed due to contributions of the TAN rings. In addition, the positive ROA signal at 1297 cm^{-1} also disappears, so that the peak in the symmetric CH_3 bending region becomes sharper and shifts to 1311 cm^{-1}. Overall, if the contributions of the TAN rings are removed, the calculated spectrum of

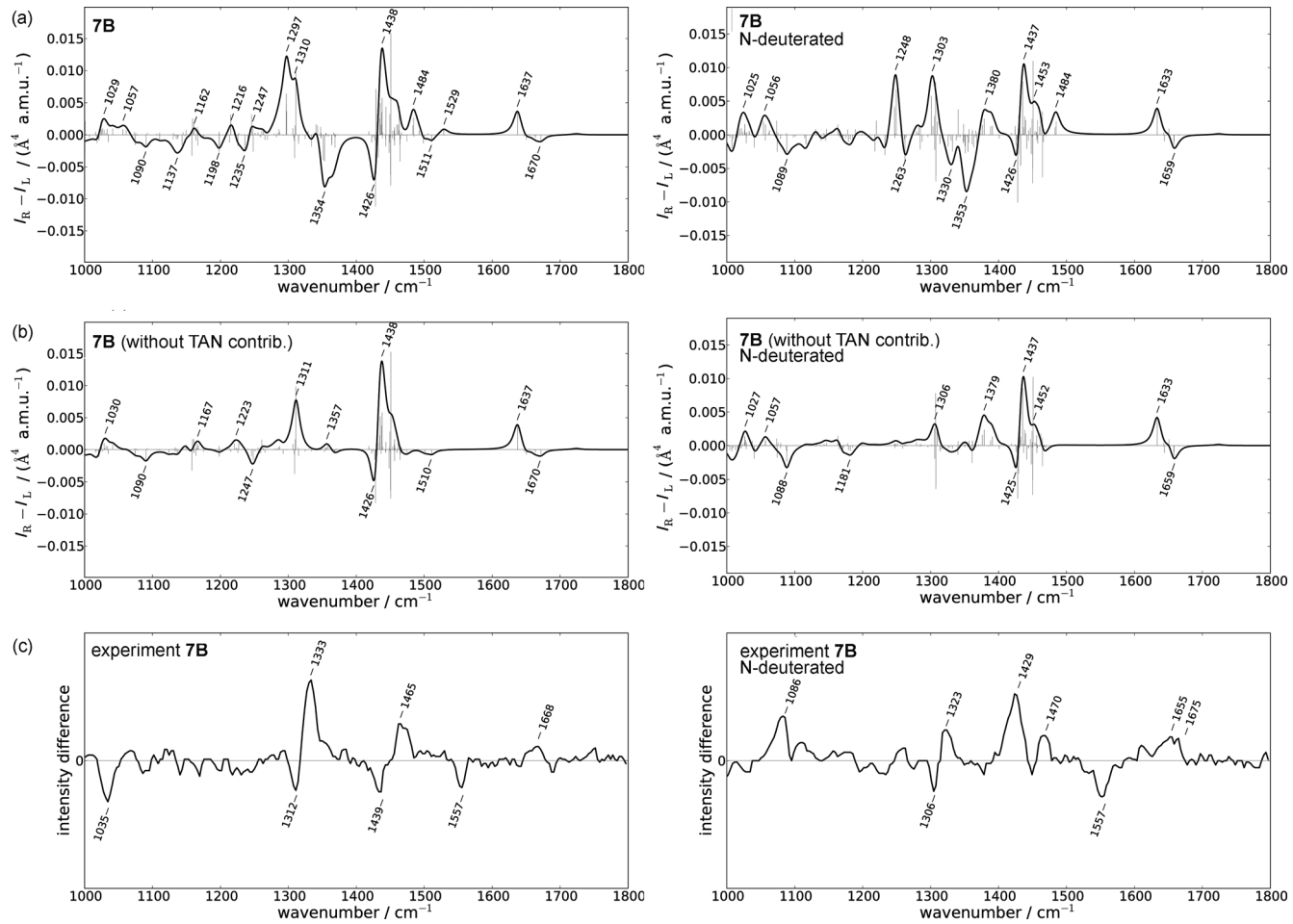

Figure 8. a) Calculated ROA spectra of the 3_{10}-helical polypeptide **7B** in the *anti*-N conformation. b) Calculated ROA spectra of **7B**, in which the contributions of the TAN rings to the ROA intensities have been removed. All calculated spectra have been plotted by using a Lorentzian line width of 15 cm^{-1} and the individual transitions have been included as a line spectrum scaled by 0.04. On the left, the spectra of the non-deuterated polypeptides are shown; on the right the spectra of the N-deuterated analogues. c) Experimental ROA spectra of **7B** in H_2O (left) and in D_2O (right). These experimental spectra have been taken from reference [49]

7B largely resembles that of the *anti*-N conformer of $(\alpha\text{-MeNva})_{10}$.

The experimental ROA spectrum of **7B** reported in reference [49] can be compared with the calculated spectra in Figure 8c (left). Before proceeding with a detailed comparison, it is important to emphasize that the calculations include several simplifications. Most importantly, solvent effects (which are important when making a comparison with a spectrum measured in aqueous solution) are not included. Moreover, the calculation only considers a single structure, even though an average of many conformers would be required. The accurate inclusion of these contributions is, however, currently still not feasible. Nevertheless, the calculations are largely consistent with the experimental spectrum. The amide I band shows a small, positive peak in both the calculation and in experiment, whereas the other amide bands are not visible. In the asymmetric CH_3 bending region, the experimental spectrum shows a broad positive peak at 1465 cm^{-1}, which can be related to the broad positive peak between 1440 and 1470 cm^{-1} in the calculated spectra. This feature can thus be assigned to the asymmetric CH_3 bending and $C^{\gamma}H_2$ scissoring vibrations, whereas the adjacent negative peak at 1439 cm^{-1} in the experimental spectrum can be assigned to the $C^{\beta}H_2$ scissoring vibrations. Moreover, the couplet in the experimental spectrum that is negative at 1312 cm^{-1} and positive at 1333 cm^{-1} has to be assigned to the in-phase combination of the CH_2 twisting vibrations because this is the only band in this region for which the calculations predict significant ROA intensity. In addition, the local-mode analysis indicated that the vibrational and intensity coupling constants obtained for this band in the most stable *anti*-N conformer were consistent with a couplet that was negative at low wavenumbers and positive at higher wavenumbers, even though the splitting between the positive and the negative peak was too small in the calculation.

In reference [49], a ROA spectrum recorded in D_2O was also reported; this is shown in the right-hand side of Figure 8c. In this case, the N–H hydrogen atoms of the peptide groups are exchanged for deuterium. The corresponding calculations for this N-deuterated variant of **7B** are included in the right-hand side of Figure 8a and b. Upon deuteration, the amide I and

asymmetric CH_3 bending bands between 1440 and 1470 cm^{-1} do not change significantly in the calculation, which agrees with the experimental observations. The in-phase CH_2 twisting band shifts slightly by 5 cm^{-1} in the calculation, whereas the corresponding couplet in the experimental spectrum shifts by 10 cm^{-1} in the same direction. This change in the position of the in-phase CH_2 twisting band results because the small contribution of the classical amide III vibration to these modes is removed. Finally, in the calculation the amide II′ band now appears at 1379 cm^{-1} and gains positive ROA intensity because it now mixes with the asymmetric CH_3 bending and the CH_2 scissoring vibrations in this region. In the experimental spectrum, this amide II′ band shows up at higher wavenumbers and overlaps with the broad positive peak at 1365 cm^{-1}. The discrepancy between experiment and the calculations for the amide II′ band can possibly be explained by solvent effects, which can be expected to have a large effect because coupling of the amide II′ vibration with side-chain vibrations depends on small changes in its position.

Finally, assignment of the negative peak at 1557 cm^{-1} in the experimental ROA spectra (in H_2O and in D_2O) is not possible. Neither vibration of the polypeptide backbone nor of the side chains (including the TAN rings) appears in this region. Therefore, neglecting solvent effects or conformational averaging from the calculations cannot account for the absence of this peak. Moreover, as concluded in reference [49], contributions from amide II or N–H vibrations of the TAN rings can be ruled out, since the position of this peak is not affected by deuteration. Thus, two possible explanations for this band remain: either it is due to an overtone or a Fermi resonance, which would require a treatment that goes beyond the harmonic approximation,[69] or it is an experimental artifact.

7. Conclusions

The reliable prediction of the ROA spectra of polypeptides is still a very challenging task. Moreover, in many cases, a mere comparison of calculated and experimental spectra is not sufficient. Instead, one should aim to identify signatures that are similar in polypeptides with a specific secondary structure by extracting general rules that determine the positions, intensities, and shapes of the bands in ROA spectra. To this end, careful analysis in terms of localized modes can be a valuable tool. Herein, the ROA spectra of a series of 3_{10}-helical polypeptides were investigated to identify how the chain length, C^{α}-substitution pattern, as well as variations of the side chains and their conformations affect the ROA spectra and possible signatures of 3_{10}-helical structures.

First, based on calculations for a 3_{10}-helical Ala_{20} polypeptide, it was previously proposed[37] that an amide I couplet that is positive at low wavenumbers and negative at high wavenumbers (opposite to the one found in α-helical polypeptides) could be used to distinguish 3_{10}-helices from α helices. Herein, it was found that, for shorter helices, this couplet disappears because the splitting between its positive and negative parts decreases. Moreover, in these shorter helices, the deviations observed at the ends of the helices altered the amide I band shape. This is in line with the experimental observation that there is no amide I couplet in the ROA spectrum of the 3_{10}-helical heptapeptide **7B**. Nevertheless, the analysis performed herein showed that the vibrational and intensity couplings responsible for the reverse amide I couplet in longer 3_{10}-helices are preserved in shorter polypeptides, even in C^{α}-tetrasubstituted polypeptides and if larger aliphatic side chains are introduced. Thus, such a reverse amide I couplet can be predicted in 3_{10}-helical polypeptides, provided their chain length is sufficient. However, in proteins there are usually only short 3_{10}-helical segments, so it might not be possible to observe such a reverse amide I couplet in protein ROA spectra.

Second, while the amide I coupling patterns are preserved in C^{α}-tetrasubstituted polypeptides, there are several large differences from C^{α}-trisubstituted polypeptides. The sign of the amide II band changes and its intensity decreases. Furthermore, in the extended amide III region the ROA spectra are altered significantly because of the absence of C^{α}-hydrogen atoms. Most importantly, the C^{α}–H bending bands disappear and the amide III band shifts to lower wavenumbers. Since there is no mixing between the classical amide III vibration and the C^{α}–H bending vibrations, the amide III band loses most of its intensity and is not visible in the ROA spectra.

Third, the effect of introducing larger aliphatic side chains on the ROA spectra, specifically in the region between about 1260 and 1470 cm^{-1}, was investigated. In particular, the scissoring vibrations of the additional CH_2 groups appear close to the asymmetric CH_3 bending vibrations and partly mix with these vibrations, whereas the CH_2 wagging and twisting vibrations are best discussed together with the symmetric CH_3 bending vibrations. One prominent feature of the considered 3_{10}-helical polypeptides is that of the symmetric CH_3 bending, CH_2 wagging, and CH_2 twisting bands in the region between 1260 and 1380 cm^{-1} only one band, the in-phase CH_2 twisting vibration, shows a significant ROA signal. Because very large intensity coupling terms are observed for this band, one obtains a strong couplet that was also identified in the experimental ROA spectrum of **7B**. Even though C^{α}-tetrasubstituted polypeptides were investigated herein, it should be emphasized that the assignments of the bands due to side-chain vibrations can be expected to be still valid for standard C^{α}-trisubstituted polypeptides and should be useful for the interpretation of their ROA spectra.

It is important to note that some of the ROA features found for the bands related to side-chain vibrations appear to be independent of the side-chain conformation. For instance, a strong ROA signal for the in-phase CH_2 twisting bands and a strong positive signal in the asymmetric CH_3 bending region were common to all of the conformers considered and can thus be related to the helical structure. However, an accurate prediction of the ROA bands due to side-chain vibrations requires a more thorough averaging over different possible conformations. By combining molecular dynamics simulations with calculation of ROA spectra, such studies are possible for small molecules.[67,70–72] However, for large molecules, such as polypeptides, more efficient methods are necessary. Analyses in terms of localized modes might allow the extraction of trans-

ferable parameters for side-chain vibrations and their ROA intensities as well as coupling terms. These could then be used to sample the ROA spectra of a larger numbers of conformers, thus going beyond simpler fragment-based approximations.[73,74]

Computational Methodology

The molecular structures of all 3_{10}-helical polypeptides considered herein were optimized by using DFT with the Turbomole program package.[75,76] The BP86 exchange-correlation functional[77,78] and Ahlrichs' valence triple-zeta basis with one set of polarization functions (TZVP)[79,80] were used throughout. All calculations were performed for the full molecular structures. Solvent effects were not included at this stage because their implicit inclusion is not sufficient and an explicit treatment renders the calculations infeasible.

Vibrational frequencies and normal modes, as well as the polarizability tensor derivatives required for the calculation of the ROA backscattering intensities were calculated by numerical differentiation with the SNF program.[55,81] The analytic energy gradients needed for the seminumerical calculation of the harmonic force field were calculated with Turbomole for distorted structures.[55,81] Vibrational frequencies were not scaled because it was shown previously that unscaled harmonic BP86 frequencies are in satisfactory agreement with experimentally observed fundamental frequencies.[82–84] This is further supported by the reasonable agreement between the ROA spectra calculated for $(Ala)_{20}$ and the experimental spectra of polyalanine.[37] The polarizability tensors required for the ROA intensities were calculated with time-dependent DFT by an extended version[85] of Turbomole's ESCF program.[86–89] To ensure gauge-invariance, the velocity representation of the electric dipole operator was employed for the $\beta(\boldsymbol{G}')^2$ invariant.[85] The ROA intensities were calculated for an excitation wavelength of 799 nm, which was well away from any electronic absorption frequency of the considered polypeptides in all cases.

For the analysis of the calculated ROA spectra, the localized modes were obtained by determining the unitary transformation of the normal modes that contributed to this band and led to optimally localized modes, according to the atomic contribution criterion.[40] The LocVib add-on package to SNF was used for the local-mode analysis. Details on the assignment of the individual normal modes to bands, which is a prerequisite for such an analysis, are given in the Supporting Information.

Pictures of molecular structures and normal modes were prepared with Jmol;[90] plots of vibrational spectra and the graphical representations of the intensity coupling matrices in the Supporting Information were produced by using the Matplotlib package.[91]

Acknowledgements

I thank Prof. Markus Reiher (ETH Zurich) for continuous support and helpful discussions. Funding from the DFG Center for Functional Nanostructures at KIT is gratefully acknowledged.

Keywords: chirality · density functional calculations · helical structures · proteins · vibrational spectroscopy

[1] O. C. Redfern, B. Dessailly, C. A. Orengo, *Curr. Opin. Struct. Biol.* **2008**, *18*, 394 – 402.
[2] P. E. Wright, H. J. Dyson, *J. Mol. Biol.* **1999**, *293*, 321 – 331.
[3] D. Röthlisberger, O. Khersonsky, A. M. Wollacott, L. Jiang, J. DeChancie, J. Betker, J. L. Gallaher, E. A. Althoff, A. Zanghellini, O. Dym, S. Albeck, K. N. Houk, D. S. Tawfik, D. Baker, *Nature* **2008**, *453*, 190 – 195.
[4] L. Jiang, E. A. Althoff, F. R. Clemente, L. Doyle, D. Röthlisberger, A. Zanghellini, J. L. Gallaher, J. L. Betker, F. Tanaka, C. F. Barbas, D. Hilvert, K. N. Houk, B. L. Stoddard, D. Baker, *Science* **2008**, *319*, 1387 – 1391.
[5] K. Wüthrich, *NMR of Proteins and Nucleic Acids*, Wiley-Interscience, New York, **1986**.
[6] R. R. Ernst, G. Bodenhausen, A. Wokaun, *Principles of Nuclear Magnetic Resonance in One And Two Dimensions*, Clarendon Press, Oxford, **1987**.
[7] Z. Ganim, H. S. Chung, A. W. Smith, L. P. DeFlores, K. C. Jones, A. Tokmakoff, *Acc. Chem. Res.* **2008**, *41*, 432 – 441.
[8] W. Zhuang, T. Hayashi, S. Mukamel, *Angew. Chem.* **2009**, *121*, 3804 – 3838; *Angew. Chem. Int. Ed.* **2009**, *48*, 3750 – 3781.
[9] P. R. Carey, *J. Biol. Chem.* **1999**, *274*, 26625 – 26628.
[10] G. J. Thomas, Jr., *Biopolymers* **2002**, *67*, 214 – 225.
[11] E. Vass, M. Hollosi, F. Besson, R. Buchet, *Chem. Rev.* **2003**, *103*, 1917 – 1954.
[12] P. Hamm, M. Lim, R. M. Hochstrasser, *J. Phys. Chem. B* **1998**, *102*, 6123 – 6138.
[13] H. Maekawa, C. Toniolo, A. Moretto, Q. B. Broxterman, N.-H. Ge, *J. Phys. Chem. B* **2006**, *110*, 5834 – 5837.
[14] L. P. DeFlores, Z. Ganim, R. A. Nicodemus, A. Tokmakoff, *J. Am. Chem. Soc.* **2009**, *131*, 3385 – 3391.
[15] H. Maekawa, M. De Poli, C. Toniolo, N.-H. Ge, *J. Am. Chem. Soc.* **2009**, *131*, 2042 – 2043.
[16] R. Schweitzer-Stenner, *J. Raman Spectrosc.* **2001**, *32*, 711 – 732.
[17] A. Cua, D. H. Stewart, M. J. Reifler, G. W. Brudvig, D. F. Bocian, *J. Am. Chem. Soc.* **2000**, *122*, 2069 – 2077.
[18] A. V. Mikhonin, Z. Ahmed, A. Ianoul, S. A. Asher, *J. Phys. Chem. B* **2004**, *108*, 19020 – 19028.
[19] I. R. Rodriguez-Mendieta, G. R. Spence, C. Gell, S. E. Radford, D. A. Smith, *Biochemistry* **2005**, *44*, 3306 – 3315.
[20] C.-Y. Huang, G. Balakrishnan, T. G. Spiro, *J. Raman Spectrosc.* **2006**, *37*, 277 – 282.
[21] L. D. Barron, A. D. Buckingham, *Chem. Phys. Lett.* **2010**, *492*, 199 – 213.
[22] T. A. Keiderling in *Circular Dichroism: Principles and Applications, 2nd ed.* (Eds.: N. Berova, K. Nakanishi, R. W. Woody), Wiley-VCH, Weinheim, **2000**, pp. 621 – 666.
[23] L. D. Barron, *Molecular Light Scattering and Optical Activity, 2nd ed.*, Cambridge University Press, Cambridge, **2004**.
[24] L. D. Barron, M. P. Bogaard, A. D. Buckingham, *J. Am. Chem. Soc.* **1973**, *95*, 603 – 605.
[25] W. Hug, S. Kint, G. F. Bailey, J. R. Scherer, *J. Am. Chem. Soc.* **1975**, *97*, 5589 – 5590.
[26] C. Herrmann, M. Reiher, *Top. Curr. Chem.* **2007**, *268*, 85 – 132.
[27] R. A. G. D. Silva, J. Kubelka, P. Bouř, S. M. Decatur, T. A. Keiderling, *Proc. Natl. Acad. Sci. USA* **2000**, *97*, 8318 – 8323.
[28] J. Kubelka, R. A. G. D. Silva, T. A. Keiderling, *J. Am. Chem. Soc.* **2002**, *124*, 5325 – 5332.
[29] I. H. McColl, E. W. Blanch, L. Hecht, N. R. Kallenbach, L. D. Barron, *J. Am. Chem. Soc.* **2004**, *126*, 5076 – 5077.
[30] J. Kapitán, V. Baumruk, P. Bouř, *J. Am. Chem. Soc.* **2006**, *128*, 2438 – 2443.
[31] L. D. Barron, L. Hecht, E. W. Blanch, A. F. Bell, *Prog. Biophys. Mol. Biol.* **2000**, *73*, 1 – 49.
[32] L. D. Barron, E. W. Blanch, L. Hecht in *Advances in Protein Chemistry, Vol. 62* (Ed.: G. D. Rose), Elsevier, San Diego, **2002**, pp. 51 – 90.
[33] L. D. Barron, L. Hecht, I. H. McColl, E. W. Blanch, *Mol. Phys.* **2004**, *102*, 731 – 744.
[34] F. Zhu, N. W. Isaacs, L. Hecht, G. E. Tranter, L. D. Barron, *Chirality* **2006**, *18*, 103 – 115.
[35] C. Herrmann, K. Ruud, M. Reiher, *ChemPhysChem* **2006**, *7*, 2189 – 2196.
[36] C. Herrmann, K. Ruud, M. Reiher, *Chem. Phys.* **2008**, *343*, 200 – 209.
[37] Ch. R. Jacob, S. Luber, M. Reiher, *Chem. Eur. J.* **2009**, *15*, 13491 – 13508.
[38] S. Luber, M. Reiher, *J. Phys. Chem. B* **2010**, *114*, 1057 – 1063.
[39] T. Weymuth, C. R. Jacob, M. Reiher, *ChemPhysChem* **2011**, *12*, 1165 – 1175.
[40] C. R. Jacob, M. Reiher, *J. Chem. Phys.* **2009**, *130*, 084106.
[41] C. R. Jacob, S. Luber, M. Reiher, *J. Phys. Chem. B* **2009**, *113*, 6558 – 6573.

[42] I. H. McColl, E. W. Blanch, L. Hecht, L. D. Barron, *J. Am. Chem. Soc.* **2004**, *126*, 8181 – 8188.
[43] L. D. Barron, L. Hecht, A. F. Bell, G. Wilson, *Appl. Spectrosc.* **1996**, *50*, 619 – 629.
[44] J. Teraoka, A. F. Bell, L. Hecht, L. D. Barron, *J. Raman Spectrosc.* **1998**, *29*, 67 – 71.
[45] C. Toniolo, E. Benedetti, *Macromolecules* **1991**, *24*, 4004 – 4009.
[46] F. Formaggio, M. Crisma, P. Rossi, P. Scrimin, B. Kaptein, Q. B. Broxterman, J. Kamphuis, C. Toniolo, *Chem. Eur. J.* **2000**, *6*, 4498 – 4504.
[47] C. Toniolo, M. Crisma, F. Formaggio, C. Peggion, *Biopolymers* **2001**, *60*, 396 – 419.
[48] F. Formaggio, M. Crisma, C. Toniolo, Q. B. Broxterman, B. Kaptein, C. Corbier, M. Saviano, P. Palladino, E. Benedetti, *Macromolecules* **2003**, *36*, 8164 – 8170.
[49] C. Toniolo, F. Formaggio, S. Tognon, Q. B. Broxterman, B. Kaptein, R. Huang, V. Setnicka, T. A. Keiderling, I. H. McColl, L. Hecht, L. D. Barron, *Biopolymers* **2004**, *75*, 32 – 45.
[50] E. B. Wilson, J. C. Decius, P. C. Cross, *Molecular Vibrations: The Theory of Infrared and Raman Vibrational Spectra*, Dover, New York, **1980**.
[51] D. A. Long, *The Raman Effect: A Unified Treatment of the Theory of Raman Scattering by Molecules*, Wiley, Chichester, **2001**.
[52] K. Ruud, T. Helgaker, P. Bouř, *J. Phys. Chem. A* **2002**, *106*, 7448 – 7455.
[53] M. Pecul, K. Ruud, *Int. J. Quantum Chem.* **2005**, *104*, 816 – 829.
[54] P. L. Polavarapu, *J. Phys. Chem.* **1990**, *94*, 8106 – 8112.
[55] J. Neugebauer, M. Reiher, C. Kind, B. A. Hess, *J. Comput. Chem.* **2002**, *23*, 895 – 910.
[56] M. Reiher, V. Liegeois, K. Ruud, *J. Phys. Chem. A* **2005**, *109*, 7567 – 7574.
[57] D. Rappoport, F. Furche, *J. Chem. Phys.* **2005**, *122*, 064105.
[58] V. Liegeois, K. Ruud, B. Champagne, *J. Chem. Phys.* **2007**, *127*, 204105.
[59] K. Ruud, A. J. Thorvaldsen, *Chirality* **2009**, *21*, E54 – E67.
[60] R. Bast, U. Ekström, B. Gao, T. Helgaker, K. Ruud, A. J. Thorvaldsen, *Phys. Chem. Chem. Phys.* **2011**, *13*, 2627.
[61] L. D. Barron, *J. Chem. Soc. A* **1971**, 2899 – 2904.
[62] Ch. R. Jacob, S. Luber, M. Reiher, *ChemPhysChem* **2008**, *9*, 2177 – 2180.
[63] T. Weymuth, C. R. Jacob, M. Reiher, *J. Phys. Chem. B* **2010**, *114*, 10649 – 10660.
[64] V. Liégeois, C. R. Jacob, B. Champagne, M. Reiher, *J. Phys. Chem. A* **2010**, *114*, 7198 – 7212.
[65] A. Lakhani, A. Roy, M. De Poli, M. Nakaema, F. Formaggio, C. Toniolo, T. A. Keiderling, *J. Phys. Chem. B* **2011**, *115*, 6252 – 6264.
[66] P. Bouř, J. Kapitan, V. Baumruk, *J. Phys. Chem. A* **2001**, *105*, 6362 – 6368.
[67] J. Kapitan, V. Baumruk, V. Kopecky, R. Pohl, P. Bouř, *J. Am. Chem. Soc.* **2006**, *128*, 13 451 – 13 462.
[68] S. Luber, M. Reiher, *J. Phys. Chem. A* **2009**, *113*, 8268 – 8277.
[69] W. Hug, J. Haesler, S. I. Kozhushkov, A. de Meijere, *ChemPhysChem* **2007**, *8*, 1161 – 1169.
[70] J. Kapitan, V. Baumruk, V. J. Kopecky, P. Bouř, *J. Phys. Chem. A* **2006**, *110*, 4689 – 4696.
[71] J. R. Cheeseman, M. S. Shaik, P. L. A. Popelier, E. W. Blanch, *J. Am. Chem. Soc.* **2011**, *133*, 4991 – 4997.
[72] K. H. Hopmann, K. Ruud, M. Pecul, A. Kudelski, M. Dračínský, P. Bouř, *J. Phys. Chem. B* **2011**, *115*, 4128 – 4137.
[73] P. Bouř, J. Sopková, L. Bednárová, P. Maloň, T. A. Keiderling, *J. Comput. Chem.* **1997**, *18*, 646 – 659.
[74] N. S. Bieler, M. P. Haag, C. R. Jacob, M. Reiher, *J. Chem. Theory Comput.* **2011**, *7*, 1867 – 1881.
[75] R. Ahlrichs, et al., Turbomole, http://www.turbomole.com.
[76] R. Ahlrichs, M. Bär, M. Häser, H. Horn, C. Kölmel, *Chem. Phys. Lett.* **1989**, *162*, 165 – 169.
[77] A. D. Becke, *Phys. Rev. A* **1988**, *38*, 3098.
[78] J. P. Perdew, *Phys. Rev. B* **1986**, *33*, 8822.
[79] A. Schäfer, C. Huber, R. Ahlrichs, *J. Chem. Phys.* **1994**, *100*, 5829 – 5835.
[80] Turbomole basis set library, ftp://ftp.chemie.uni-karlsruhe.de/pub/basen.
[81] J. Neugebauer, C. Herrmann, S. Luber, M. Reiher, SNF 4.0—A Program for the Quantum Chemical Calculation of Vibrational Spectra, http://www.reiher.ethz.ch/software/snf.
[82] G. Brehm, M. Reiher, S. Schneider, *J. Phys. Chem. A* **2002**, *106*, 12024 – 12034.
[83] M. Reiher, G. Brehm, S. Schneider, *J. Phys. Chem. A* **2004**, *108*, 734 – 742.
[84] G. Brehm, M. Reiher, B. Le Guennic, M. Leibold, S. Schindler, F. W. Heinemann, S. Schneider, *J. Raman Spectrosc.* **2006**, *37*, 108 – 122.
[85] S. Luber, M. Reiher, *Chem. Phys.* **2008**, *346*, 212 – 223.
[86] R. Bauernschmitt, R. Ahlrichs, *Chem. Phys. Lett.* **1996**, *256*, 454 – 464.
[87] R. Bauernschmitt, M. Häser, O. Treutler, R. Ahlrichs, *Chem. Phys. Lett.* **1997**, *264*, 573 – 578.
[88] F. Furche, R. Ahlrichs, *J. Chem. Phys.* **2002**, *117*, 7433 – 7447.
[89] S. Grimme, F. Furche, R. Ahlrichs, *Chem. Phys. Lett.* **2002**, *361*, 321 – 328.
[90] Jmol—An Open-Source Molecule Viewer, http://jmol.sourceforge.net.
[91] Matplotlib—A Python 2D Plotting Library, http://matplotlib.sourceforge.net/.

Received: July 31, 2011
Published online on November 3, 2011

